The fabrication of Schottky photodiode by monolayer graphene direct-transfer-on-silicon

The fabrication of Schottky photodiode by monolayer graphene direct-transfer-on-silicon

Yiming Wang [a, b], Shuming Yang [a, *] Alberto Ballesio [b], Matteo Parmeggiani [b,c], Alessio Verna [b], Matteo Cocuzza [b,d], Candido Fabrizio Pirri [b,c], Simone Luigi Marasso [b,d]

[a] State Key Laboratory for Manufacturing System Engineering, Xi'an Jiaotong University, Xi'an, Shaanxi, 710049, China.

[b] Chilab - Materials and Microsystems Laboratory, DISAT, Politecnico di Torino - Via Lungo Piazza d'Armi 6, IT 10034, Chivasso (Turin), Italy

[c] Center for Sustainable Future Technologies, Italian Institute of Technology, Corso Trento 21, IT 10129 Turin, Italy

[d] CNR-IMEM, Parco Area delle Scienze 37a, IT 43124, Parma, Italy

*e-mail:shuming.yang@mail.xjtu.edu.cn

Abstract

Two-step hot embossing process was used to transfer graphene and to fabricate Gr/Si Schottky photodiodes. As a direct graphene transfer technique, through a hot embossing system, CVD Gr monolayer was transferred from copper foil to Cyclic Olefin Copolymer (COC) foil without PMMA sacrificial layer. Then hot embossing was employed once again to bond graphene with the prepared Si substrate to form Schottky contact. Electrical and photoelectrical characterizations have been performed to evaluate the Schottky photodiode. The photocurrent increase linearly with light intensity under 633 nm illumination. With an appropriate bias voltage, the maximum responsivity reaches 0.73 A/W. Extracted from I-V characteristics by Cheung's function, the Schottky barrier height and ideality factor are 1.01 eV and 2.66, respectively. The experimental result shows the feasibility and effectiveness of this hot embossing fabrication process, which demonstrates the opportunity for large scale production and provides a new approach for graphene optoelectronics.

∗ Corresponding author. E-mail address: shuming.yang@mail.xjtu.edu.cn.

Keywords: hot embossing, graphene transfer, graphene photodetector, graphene silicon Schottky.

1. Introduction

Graphene photodetectors have experienced rapid development in the past decade, owing to the unique electrical and optical properties of graphene, like high charge carrier mobility and wide spectrum light absorption[1]. As we know, graphene, the first truly two-dimensional material[2], was successfully obtained by mechanical exfoliation method, which is lowly efficient and not suitable for mass production[3]. Since then, many efforts have been devoted to effective synthesis of high-quality graphene[4-7]. From the developing trends over recent years[8], chemical vapor deposition (CVD) is the most promising one among all others methods to obtain monolayers for integration in large scale device production. However, the CVD growth needs metal seed layer like Cu and Ni and, hence, graphene transfer technologies became the key point between synthesis and application[9-12]. The most frequently used graphene transfer method is based on a PolyMethylMethAcrylate (PMMA) sacrificial layer and metal etching processes, but it suffers from the residues of PMMA and it is hard to scale to large area and match the semiconductor manufacturing compatibility.

Graphene/Silicon (Gr/Si) Schottky junction is one of the most important components of graphene based photosensitive devices. In Gr/Si Schottky photodiode, the incident light passes through the graphene layer and the photons are absorbed by silicon to excite electron-hole pairs. During this process, graphene collects the photo-generated carriers and provides a high speed pathway for carriers transport[1]. Since Li et al. transferred the CVD graphene on HF etched n-type Si wafer[13], Gr/Si photoelectrical devices has attracted great attention[14-17].

The most frequently used method to fabricate Gr/Si Schottky devices uses PMMA as a sacrificial media layer to transfer graphene from original metal substrate to silicon substrate[17-21]. In this traditional method, PMMA solution with a certain concentration is spin-coated on graphene/metal substrate and heated to evaporate the solvent to form a PMMA layer. After

etching the metal substrate by copper etching solution (usually $FeCl_3$, sometimes $(NH_4)_2S_2O_8$), the PMMA/graphene floating over the air-liquid interface is picked up by silicon substrate and form Gr/Si Schottky contact. However, it is a manual procedure to pick up graphene from liquid surface to desired substrate, which cannot match the semiconductor manufacturing compatibility and, on the other hand, causes wrinkles and folds of graphene film in the handcraft. As a sacrificial media, PMMA should be removed after graphene transferring, but the PMMA residue is major problem exercising the minds of scientists around the world. The residue trap the photogenerated charge carriers when they move through the interface, causing an increase of electron/holes recombination and the degradation of device performance[17]. To solve this problem, deep UV treatment[18,19], Ar Ion Beam[20], low molecular weight PMMA[21], etc. were used to reduce the PMMA residues, while the processes became more complicated.

Hot embossing is a cost-effective and flexible fabrication technology which has been widely used for micro-/nano- fabrication, but it has been used only recently to transfer CVD grown graphene[22]. By applying this novel method, CVD grown graphene was successfully transferred from copper foil to Cyclic Olefin Copolymer (COC) foil without PMMA sacrificial layer. The hot embossing process avoids the residues of PMMA and simplifies the processing steps, thus providing the opportunity for large scale production. As a widely used technique, hot embossing has good processing compatibility to micro-/nano- manufacturing and it does not need careful operation, which is a significant advantage of this method compared with other PMMA-free graphene method[11,23,24]. The success of hot embossing graphene transferring benefits from the nature of the polymer material, which is flexible and able to contact well with graphene on original metal substrate under a certain pressure and temperature. As a result, this method was mainly used to fabricate flexible graphene device, while at present there is no attempt on graphene device on hard substrate by this method.

In this work, hot embossing process was employed twice to transfer graphene and fabricate Gr/Si Schottky photodiodes. As a direct graphene transfer technique, CVD monolayer

graphene was transferred by hot embossing from copper foil to COC foil without PMMA sacrificial layer[22]. The SiO_2/Si substrate with square window oxide layer and front and backside electrodes was prepared by photolithography, e-beam evaporation and wet etching. Then hot embossing was employed once again to bond graphene/COC with as-prepared substrate form Schottky contact in the window of insulating layer. Considering the good high transparency of COC material, the COC foil remains on the top of photodiode and protects graphene from external pollution. The incident light goes through transparent COC and graphene layer, and finally excites electron–hole pairs in silicon, which is the origin of photoelectrical response of Gr/Si Schottky diode. This paper demonstrates this new strategy to fabricate Gr/Si Schottky photodiode. We also investigate the photo response using a 633nm laser at different intensity and evaluate the relevant parameters using the thermionic emission model and the Cheung's method, which reveals that the Gr/Si Schottky diode fabricated by hot embossing has equivalent or even better performance as those fabricated by traditional method.

2. Experimental

2.1 Graphene growth and transferring to COC

After rinsing Cu foils in 10% HCl for 15 min, single layer graphene was grown on them in a CVD system (Moorfield NanoCVD 8G). The Gr/Cu was then hot embossed onto a COC foil (140 μm, TOPAS 8007 × 04). This process was performed with a hot embossing system (model HEX01JENOPTIK Mikrotechnik) with the temperature of 80 °C and the applied force of 10,000 N for 120 seconds. Since the surface was 2 cm×2 cm, the pressure was 25 MPa. Then the Cu layer was wet etched by $FeCl_3$ solution and the samples were rinsed in deionized (DI) water to remove $FeCl_3$ residues, thus graphene on COC was obtained.

2.2 Fabrication of Gr/Si Schottky photodiode

N-type Si (100) wafer (1–10 Ω cm) with 300 nm SiO_2 was used as the substrate for the fabrication of Schottky junction. Firstly, the SiO_2 layer on the backside was removed by HF etching, and Ti/Au (20nm/80nm) was deposited by e-beam evaporation to form ohmic contact. After that, Cr/Au (20nm/80nm) electrode was patterned and evaporated on the front side of SiO_2/Si wafer. Photolithography was used to define a square window on the substrate (1.6mm× 1.6mm), followed by a wet etching process in buffered oxide etch (BOE) solution to remove SiO_2 layer. Then hot embossing was used once again to bond graphene with the prepared silicon substrate to form Schottky contact in the window, which was the active area of this photodetector.

2.3 Raman, electrical and photoelectrical characterizations

Raman microscope (Renishaw plc, Wotton-under-Edge, UK) with a 532nm laser and a Leica DMLM microscope was used to characterize the graphene transferred by hot embossing process. The spectrum of COC foil was obtained in advance and was taken off from that of graphene on COC to get the contribution of graphene alone.

Keysight B2912A Source/Measure unit was used for electrical characterizations, and photoelectrical characterization was carried out under dark and 633 nm illumination with a semiconductor laser (laser power has been calibrated with Sanwa LP-1 before the measurements). Based on the thermionic emission theory, the ideality factor and Schottky barrier height were extracted from current-voltage curve to evaluate the property of Gr/Si Schottky diode.

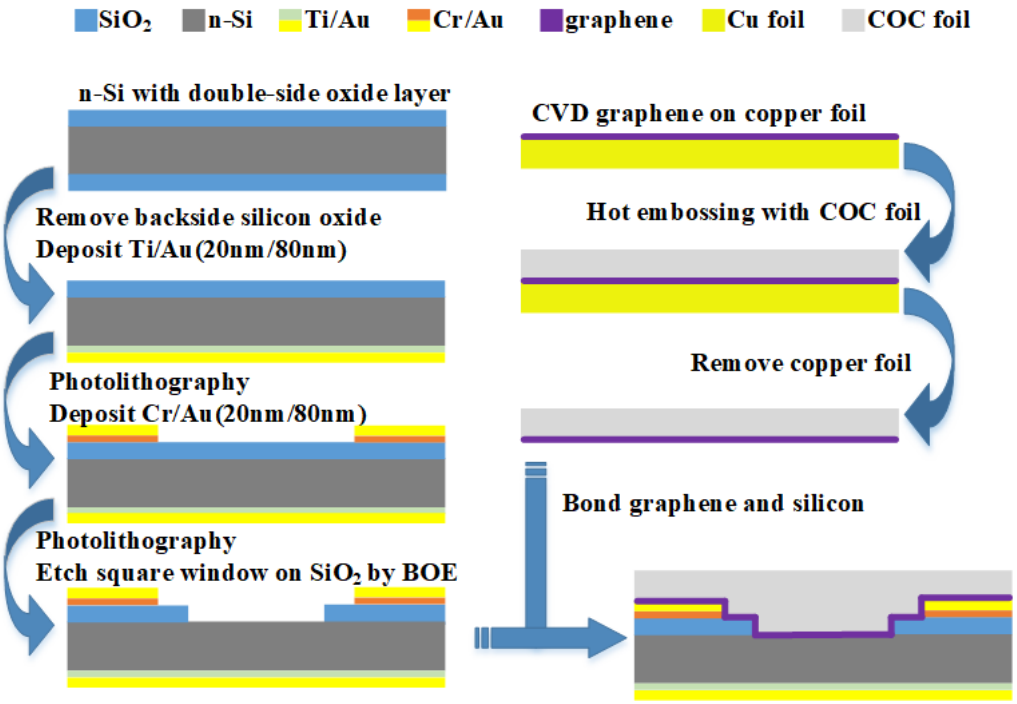

FIG. 1. Fabrication process of hot embossing transferred Gr/Si Schottky photodiode

3. Results and discussion

The Raman spectrum of the graphene transferred on COC foil by hot embossing (Fig.2) shows three main peaks: D peak at 1346 cm^{-1}, G peak at 1582 cm^{-1}, 2D peak at 2678 cm^{-1}. The 2D peak is sharp and symmetric, the full width at half maximum of the 2D peak is 35 cm^{-1} and the intensity ratio of the 2D peak to the G peak is 1.75. The shape of the peaks and the intensity ratio indicate the monolayer nature of this graphene thin film[25-27]. From the Raman spectrum it can be seen that the graphene structure is well preserved after experiencing the 25 MPa molding pressure during hot embossing process.

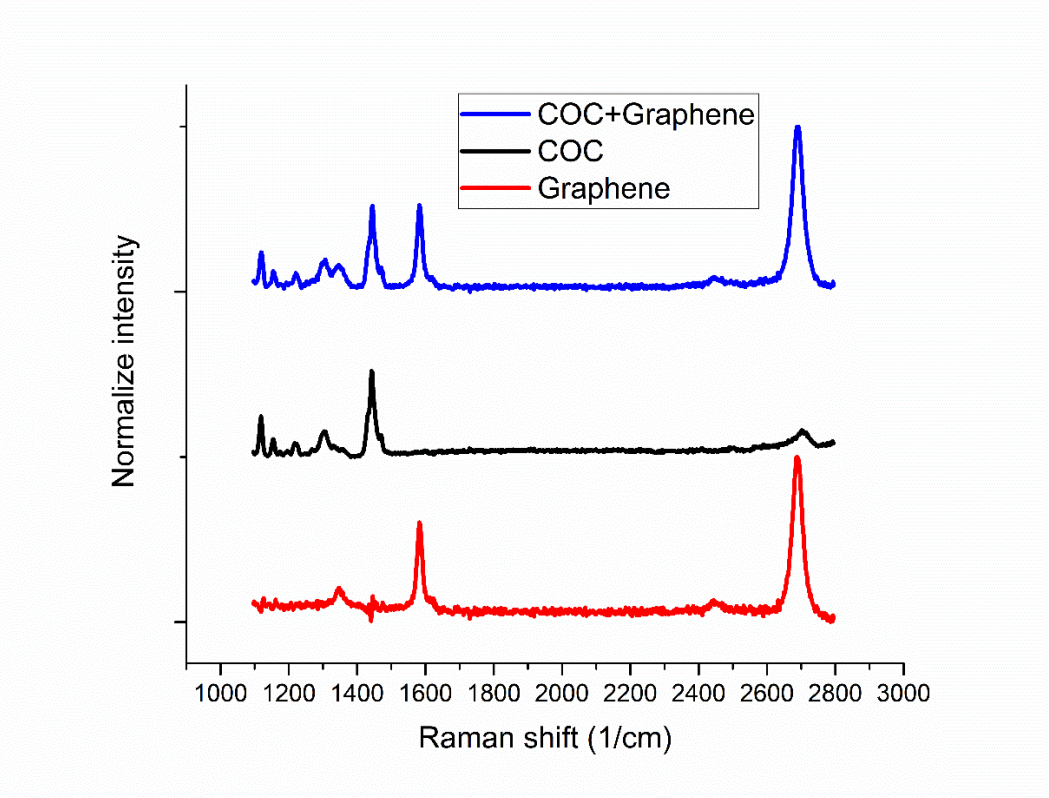

FIG. 2. Raman spectrum of hot embossing transferred graphene

As shown in Fig.3(a), I–V measurements were carried out under different incident light intensity from 0 to 15 mW/cm^2. The curves exhibit typical rectifying behavior and Gr/Si Schottky junction works in the backward voltage segment, which is similar to that of a metal/semiconductor Schottky diode. From the family of I−V curves we can see that the photocurrent of the device is highly dependent on the bias voltage: for a certain incident light power, the photocurrent rises with the increase of reverse bias and saturates at higher reverse bias. This phenomenon origins for the photovoltaic characteristic of Gr/Si Schottky junction, which can be understood from the energy band diagram as shown in Figure 4. At the graphene/silicon interface, the incident photons are absorbed by silicon and excite electron–hole pairs, which are separated by the built-in potential and transported efficiently to the external electrode under the appropriate biases, where graphene acts as a carrier collector and a high-speed channel for photo-generated carriers. While the built-in potential, Φ_i, is related to the bias voltage, as shown in Figure 4(b), the ability of charge separation can be tuned by the bias and a

relatively large built-in potential is favorable for injecting all of the photoexcited holes from silicon to graphene and obtaining the saturated photocurrent.

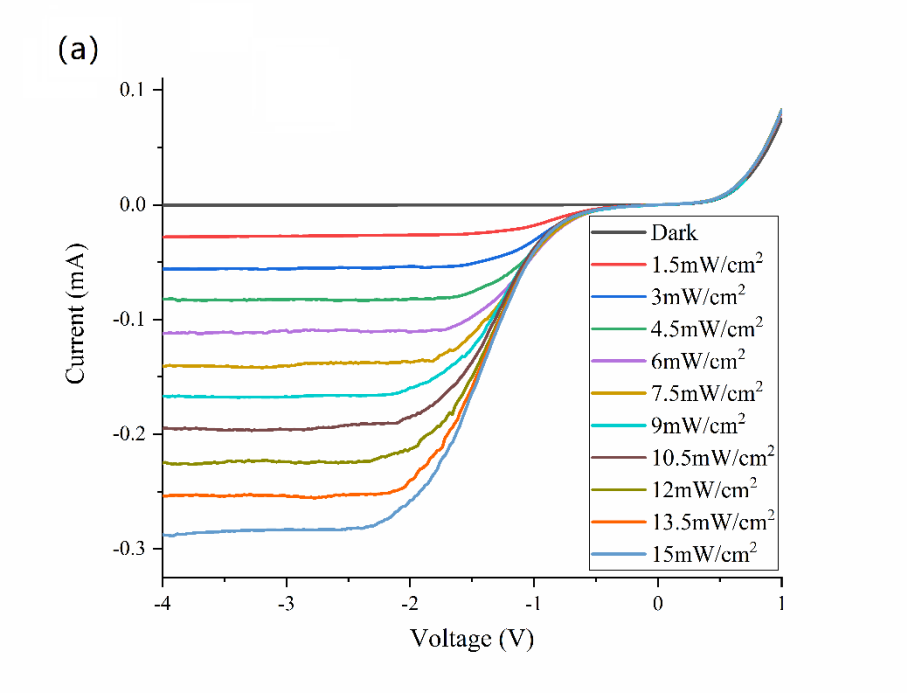

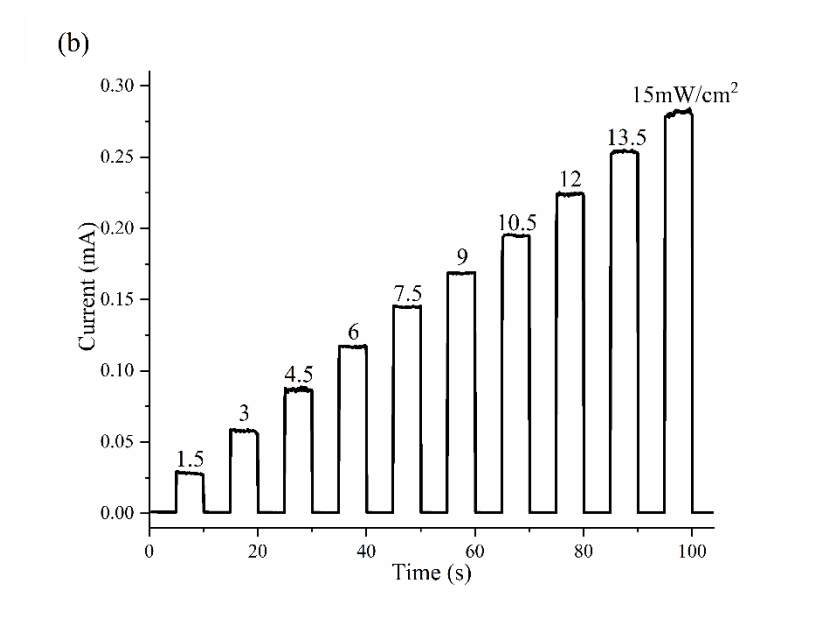

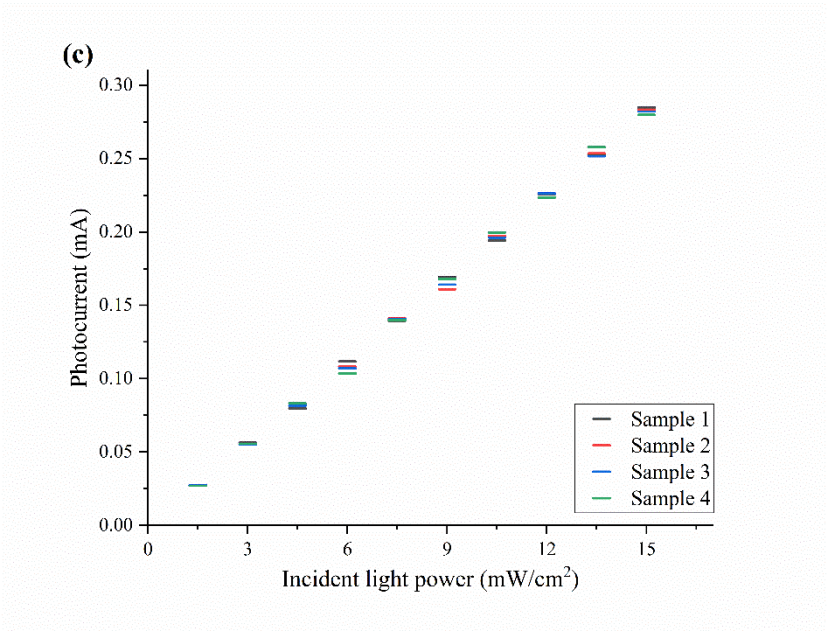

FIG. 3. (a) Current-voltage curve of Gr/n-Si Schottky photodiode under various incident light powers. (b) Time dependent photocurrent response. (c) Photocurrent of different samples under various incident light power.

While an appropriate reverse bias is applied on the Gr/Si Schottky junction, the saturated photocurrent increases linearly with the incident light intensity. Figure 3(b) displays the time dependent photoresponse to a pulse optical signal of various intensity with the reverse bias voltage of -3V, which shows the reliability and stability of the hot embossing fabricated Gr/Si photodiode. The responsivity of the hot embossing Gr/n-Si Schottky photodiode was measured to be 0.73 A/W. Four samples have been fabricated using the same processes, and their photo responses were measured under various incident light power with a reverse bias voltage of 3V. As shown in Figure 3(c), their photocurrents are almost same under same incident light power, which indicates the stability and reliability of the two-step hot embossing process.

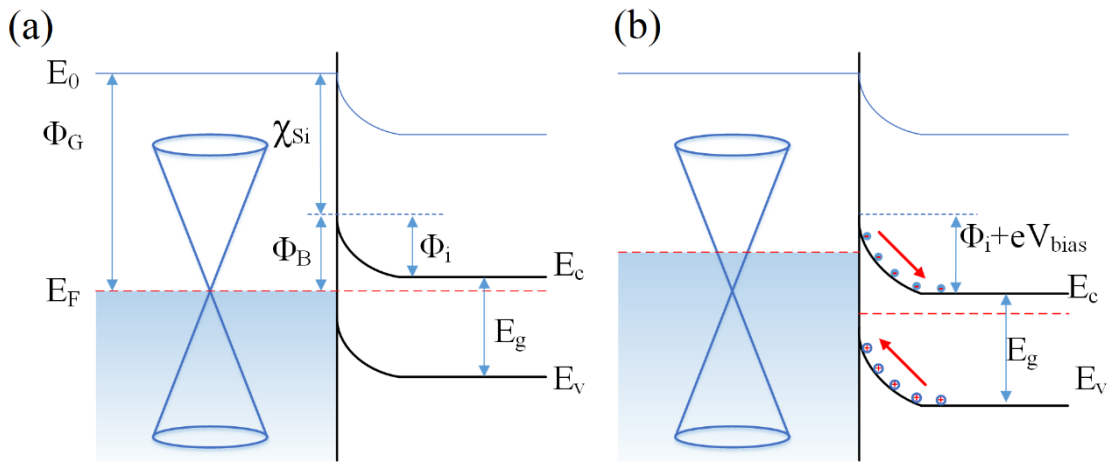

FIG. 4. Energy band diagram of the Gr/Si Schottky junction. (a) Thermal equilibrium energy band diagram of the heterojunction in darkness. (b) Reverse bias under illumination. E_c, E_v, E_F, E_g, Φ_G, χ_{Si}, Φ_B, Φ_i denote conduction band, valence band, Fermi level, bandgap, work function of graphene, electron affinity of silicon and Schottky barrier height, built-in potential, respectively

To further investigate the hot embossing Gr/Si Schottky photodiode, the key Schottky parameters were extracted from current-voltage measurement. The current–voltage relationship of Gr/n-Si junction can be described by the thermionic emission theory,

$$I = I_0\left(e^{\frac{qV}{\eta kT}} - 1\right) \quad (1)$$

where η is the ideality factor, I_0 is the saturation current defined by

$$I_0 = AA^*T^2e^{-\frac{\Phi_B}{kT}} \quad (2)$$

where A, A* and Φ_B are respectively the diode area, Richardson constant and zero-bias barrier height. When considering the effect of series resistance (R_s), V in the Eq. (1) can be replaced by the difference of the total voltage drop of the system and the voltage drop of series resistance, and two new equations can be derived from it,

$$\frac{\partial V}{\partial(\ln I)} = \frac{\eta kT}{q} + R_sI \quad (3)$$

$$H(I) = IR_s + \eta\Phi_B \quad (4)$$

where H(I) is given by

$$H(I) = V - \eta\left(\frac{kT}{q}\right)\ln\left(\frac{I}{AA^{*}T^{2}}\right) \quad (5)$$

Accordingly, the experimental values of ideality factor η, series resistance R_s and Schottky barrier height Φ_B can be extracted from the non-linear region of the forward bias I-V characteristics by Cheung's functions[28,29]

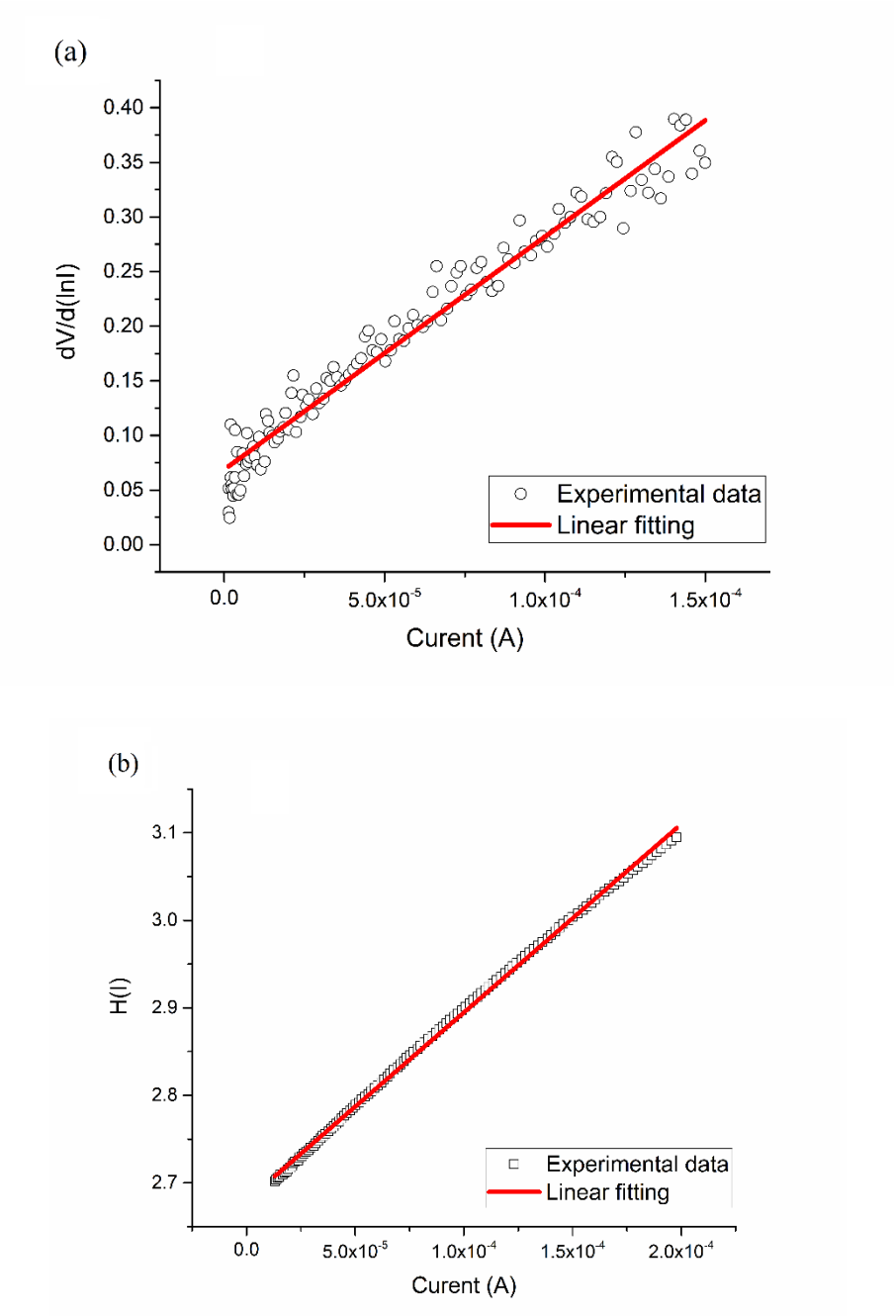

FIG. 5. Plots of dV/d(ln I) versus I (a), and H(I) versus I (b) for the Gr/Si Schottky diode.

Plots of dV/d(lnI) versus I and H(I) versus I for the Gr/Si Schottky diode are presented in Fig. 5. From the plot of dV/d(lnI)-I (Fig. 5(a)), the values of series resistance and ideality factor

are determined to be 2132 Ω and 2.66 from the intercept and slope of the forward bias. Using the ideality factor value obtained from dV/d(lnI)–I plot, the Schottky barrier height is estimated by Eq. (4) from the H(I)-I plot (Fig. 5(b)).Φ_B and R_s are found to be 1.01 eV and 2153 Ω. The R_s values obtained from the both plots are almost the same, which can be attributed to the consistency of Cheung's functions[29].

Table 1 lists the performances of graphene based photodetectors, most of them are graphene/silicon Schottky structure, some surface modified graphene devices and graphene heterojunction with other materials are also included, it can be seen that the hot embossing fabricated Gr/Si shows the same level of photo detecting ability with the ones already published.

Table 1. Summary of the performances of the graphene based photodetectors

Device structure	Responsivity	Schottky barrier height	Series resistance	Ideality factor	Reference
Graphene/Si	0.73 A/W	1.01 eV	~2100 Ω	2.66	this work
Graphene/Si	0.73 A/W	—	—	—	[1]
Graphene/Si	0.23 A/W	0.66 eV	6700 Ω	1.52	[30]
Graphene/Si	0.435 A/W	—	—	—	[31]
Graphene/Si	0.140 A/W	0.79 eV	32.1 Ω	2.24	[14]
Graphene/Si	0.214 A/W	0.79 eV	—	2.1	[15]
Graphene/Si	0.152 A/W	—	—	—	[16]
Graphene/Si	0.142 A/W	0.79 eV	14.9 Ω	—	[17]
Graphene/Si	0.24 A/W	—	—	—	[32]
Gr/Si-tips junction	2.5 A/W	0.36 eV	4500 Ω	—	[33]
PEDOT-Graphene/Si	0.172 A/W	—	—	—	[16]
P3HT–Graphene/Si	0.78 A/W	—	—	—	[32]
TFSA-Graphene/Si	0.252 A/W	0.89 eV	10.3 Ω	—	[17]
MoO3-Graphene/Si	0.4 A/W	0.86 eV	17.1 Ω	1.3	[14]
Graphene/GO/Si	0.266 A/W	0.81 eV	—	2.6	[15]
Graphene/metal	0.225 A/W	—	—	—	[34]
Graphene/Ge	0.0518 A/W	—	—	—	[35]

In a Schottky photodiode, photogenerated electron-hole pairs are separated by a built-in electric field associated with the Schottky barrier[36-38], thus the responsivity of 0.73 A/W was obtained with the high Schottky barrier height of 1.01 eV. However, in the meantime, the series

resistance reaches more than 2 kΩ, which is higher than the traditional Gr/Si photodiode fabricated by PMMA graphene transfer[1,14]. The high series resistance may attribute to the scratch or tear of graphene near to the edge of silicon window, in which a 300nm high silicon oxide step locates. The high ideality factor also indicates that the complex interface causes a negative impact on the device performance. In spite of this, the sensitive, quick and stable photo response show the feasibility and effectiveness of this hot embossing fabrication process, which provides a new approach for graphene devices.

4. Conclusion

In conclusion, a straightforward fabrication method of Gr/Si Schottky photodiode via hot embossing process has been successfully developed. Hot embossing process was used both to transfer CVD graphene from copper to COC, and to bond graphene with Si substrate to form Schottky contact. The responsivity of this Gr/Si photodiode reaches 0.73 A/W under 633 nm illumination with a reverse bias of -3V, which can be attributed to the high Schottky barrier height. Overall, this straightforward method allows to fabricate graphene based devices efficiently, and demonstrates the opportunity for large scale production.

Acknowledgements

The present work was performed in the framework and financed by POLITO BIOMed LAB, an interdepartmental laboratory financed by Politecnico di Torino and DEFLeCT ("Advanced platform for the early detection of not small cells lung cancer", Piedmont "Health & WellBeing" Platform) project. DEFLeCT project was funded by Regione Piemonte POR-FESR 2014-2020.

The authors would like to thank the supports by National Natural Science Foundation of China (No. 51575440), National Science Fund for Excellent Young Scholars (No. 51722509), National Key R&D Program of China (2017YFB1104700), and China Scholarship Council.

Data Availability

The data that support the findings of this study are available from the corresponding author upon reasonable request.

References

[1] X. Li, M. Zhu, M. Du, Z. Lv, L. Zhang, Y. Li, Y. Yang, T. Yang, X. Li, and K. Wang, Small **12,** 595-601 (2016).
[2] X. Wang, Z. Cheng, K. Xu, H. K. Tsang, and J. Xu, Nature Photonics **7,** 888 (2013).
[3] K. S. Novoselov, A. K. Geim, S. Morozov, D. Jiang, M. I. Katsnelson, I. Grigorieva, S. Dubonos, and A. A. Firsov, nature **438,** 197-200 (2005).
[4] D. Geng, H. Wang and G. Yu, Advanced Materials **27,** 2821-2837 (2015).
[5] D. Q. McNerny, B. Viswanath, D. Copic, F. R. Laye, C. Prohoda, A. C. Brieland-Shoultz, E. S. Polsen, N. T. Dee, V. S. Veerasamy, and A. J. Hart, Scientific reports **4,** 5049 (2014).
[6] A. Mohsin, L. Liu, P. Liu, W. Deng, I. N. Ivanov, G. Li, O. E. Dyck, G. Duscher, J. R. Dunlap, and K. Xiao, Acs Nano **7,** 8924-8931 (2013).
[7] F. Han, S. Yang, W. Jing, K. Jiang, Z. Jiang, H. Liu, and L. Li, Applied surface science **314,** 71-77 (2014).
[8] G. Deokar, J. Avila, I. Razado-Colambo, J. Codron, C. Boyaval, E. Galopin, M. Asensio, and D. Vignaud, Carbon **89,** 82-92 (2015).
[9] X. Chen, Z. Liu, C. Zheng, F. Xing, X. Yan, Y. Chen, and J. Tian, Carbon **56,** 271-278 (2013).
[10] L. Gao, G. Ni, Y. Liu, B. Liu, A. H. C. Neto, and K. P. Loh, Nature **505,** 190-194 (2014).
[11] G. Zhang, A. G. Gu¨ell, P. M. Kirkman, R. A. Lazenby, T. S. Miller, and P. R. Unwin, ACS applied materials & interfaces **8,** 8008-8016 (2016).
[12] Y. Fan, K. He, H. Tan, S. Speller, and J. H. Warner, Chemistry of Materials **26,** 4984-4991 (2014).
[13] X. Li, H. Zhu, K. Wang, A. Cao, J. Wei, C. Li, Y. Jia, Z. Li, X. Li, and D. Wu, Advanced materials **22,** 2743-2748 (2010).
[14] D. Xiang, C. Han, Z. Hu, B. Lei, Y. Liu, L. Wang, W. P. Hu, and W. Chen, Small **11,** 4829-4836 (2015).
[15] L. Yang, X. Yu, M. Xu, H. Chen, and D. Yang, Journal of Materials Chemistry A **2,** 16877-16883 (2014).
[16] T. Feng, D. Xie, Y. Lin, H. Zhao, Y. Chen, H. Tian, T. Ren, X. Li, Z. Li, and K. Wang, Nanoscale **4,** 2130-2133 (2012).
[17] X. Miao, S. Tongay, M. K. Petterson, K. Berke, A. G. Rinzler, B. R. Appleton, and A. F. Hebard, Nano letters **12,** 2745-2750 (2012).
[18] M. Jang, T. Q. Trung, J. Jung, B. Kim, and N. Lee, Physical Chemistry Chemical Physics **16,** 4098-4105 (2014).
[19] A. Suhail, K. Islam, B. Li, D. Jenkins, and G. Pan, Applied Physics Letters **110,** 183103 (2017).
[20] K. S. Min, K. S. Kim, K. N. Kim, A. Mishra, and G. Y. Yeom, Journal of nanoscience and nanotechnology **14,** 9108-9113 (2014).
[21] S. Kim, S. Shin, T. Kim, H. Du, M. Song, C. Lee, K. Kim, S. Cho, D. H. Seo, and S. Seo, Carbon **98,** 352-357 (2016).
[22] A. Ballesio, M. Parmeggiani, A. Verna, F. Frascella, M. Cocuzza, C. F. Pirri, and S. L. Marasso, Microelectronic Engineering **209,** 16-19 (2019).
[23] W. Lin, T. Chen, J. Chang, J. Taur, Y. Lo, W. Lee, C. Chang, W. Su, and C. Wu, ACS Nano **8,** 1784-1791 (2014).
[24] S. Cha, M. Cha, S. Lee, J. H. Kang, and C. Kim, Scientific Reports **5,** 17877 (2015).
[25] R. Liu, X. W. Fu, J. Meng, Y. Q. Bie, D. P. Yu, and Z. M. Liao, Nanoscale **5,** 5294-8 (2013).
[26] Z. Ni, Y. Wang, T. Yu, and Z. Shen, Nano Research **1,** 273-291 (2008).
[27] D. P. Yu, Advanced Materials **23,** 3938-3943 (2011).
[28] S. K. Cheung and N. W. Cheung, Applied Physics Letters **49,** 85-87 (1986).
[29] L. D. Rao, K. S. Latha, V. R. Reddy, and C. Choi, Vacuum **119,** 276-283 (2015).
[30] S. Riazimehr, D. Schneider, C. Yim, S. Kataria, V. Passi, A. Bablich, G. S. Duesberg, and M. C. Lemme, in *Spectral sensitivity of a graphene/silicon pn-junction photodetector*, 2015 (IEEE), p. 77-80.
[31] X. An, F. Liu, Y. J. Jung, and S. Kar, Nano Lett **13,** 909-16 (2013).
[32] H. Aydın, S. B. Kalkan, C. Varlikli, and C. Çelebi, Nanotechnology **29,** 145502 (2018).
[33] A. Di Bartolomeo, G. Luongo, L. Iemmo, F. Urban, and F. Giubileo, IEEE Transactions on Nanotechnology **17,** 1133-1137 (2018).

[34] S. Cakmakyapan and M. Jarrahi, in *High responsivity and bias-free graphene photodetector with nano-grating contact electrodes*, 2018 (OSA), p. 1-2.
[35] L. Zeng, M. Wang, H. Hu, B. Nie, Y. Yu, C. Wu, L. Wang, J. Hu, C. Xie, F. Liang, and L. Luo, ACS Applied Materials & Interfaces **5,** 9362
-9366
(2013).
[36] X. Liu, X. W. Zhang, Z. G. Yin, J. H. Meng, H. L. Gao, L. Q. Zhang, Y. J. Zhao, and H. L. Wang, Applied Physics Letters **105,** 183901 (2014).
[37] S. Shafique, S. Yang, Y. T. Woldu, and W. Yiming, Sensors & Actuators A Physical **288,** 107-116 (2019).
[38] S. Shafique, S. Yang, Y. Wang, Y. T. Woldu, B. Cheng, and P. Ji, Sensors and Actuators A: Physical **296,** 38-44 (2019).